Astronomy & Astrophysics manuscript no. output
February 11, 2023

Improved photometry of the hot Jupiter WASP-135b

A new analysis of the transit light curves using data from TESS and TASTE

V. Campobasso[1], A. Fahlman[1], and I. E. Karaaslan[1]

[1] Dipartimento di Fisica e Astronomia (DFA), Università degli studi di Padova
e-mail: valerio.campobasso@studenti.unipd.it, e-mail: alexanderpaul.fahlman@studenti.unipd.it,
e-mail: idilezgi.karaaslan@studenti.unipd.it

Received February 12, 2023; accepted February 16, 2023

ABSTRACT

Context. An ever growing number of surveys are collecting data on exoplanetary and potential exoplanetary systems that need to be analyzed to detect the presence of exoplanets and characterize these systems. TESS (Transiting Exoplanet Survey Satellite) and TASTE (The Asiago Search for Transit timing variation of Exoplanets) are two such surveys that observe exoplanet transits.
Aims. Our goal was to characterize the planetary system around the sun-like star WASP-135 using these two data sets. Parameters for this system exist in the literature but not with the full set of parameters found here from these instruments.
Methods. We processed raw images into light curves for the star WASP-135 and its one known hot Jupiter WASP-135b. The light curves for this system from both surveys were flattened and the transit of the exoplanet was extracted for analysis. We also found limb darkening coefficients for WASP-135 in order to improve the accuracy of the Bayesian estimation performed using the **PyORBIT** package we used to characterize the system.
Results. Parameter values found for the system include, but are not limited to: planetary radius, orbital period, impact parameter, eccentricity, and semi-major axis. WASP-135b was found to have period and radius for the two surveys of $P = (1.401378 \pm 0.000001)$ d and $R = (1.293538 \pm 0.07)\, R_{Jup}$ for TESS, and $P = (1.401378 \pm 0.000001)$ d and $R = (1.225463 \pm 0.07)\, R_{Jup}$ for TASTE.

Key words. WASP-135b – hot Jupiter – transit light curve

1. Introduction

As the number of the known exoplanets increases on a daily basis, exceeding several thousands, so does the need to characterize them according to common properties and evolutionary patterns. Back to the time when only the planets around the Sun were known, the common idea was to expect the smaller rocky planets to be placed relatively close to their hosting star, while a few gas giants would orbit further away. The discovery of the first so-called hot Jupiter (Mayor and Queloz 1995), deeply shocked the astronomical community, since no Solar System analogue existed, and it was not clear how such a huge planet could form this close to its star. Since then, different evolutionary pathways have been proposed, involving smooth migration due to dissipative planet-disk interactions (Kley and Nelson 2012), violent migration due to either planet-planet scattering or the Lidov-Kozai mechanism (Beaugé and Nesvorný 2012; Naoz et al. 2013), or in-situ formation (Batygin and Brown 2016). However, the picture is still far from being completely understood.

Nevertheless, hot Jupiters are an important class of exoplanets, being the only ones for which accurate measurements of both mass and radius can be made. Additionally, they are the perfect targets for studying atmospheric compositions using the transit spectroscopy technique. They also show interesting properties, still under investigation. For example, it has been observed (Fortney and Nettelmann 2009; Baraffe et al. 2009; Spiegel and Burrows 2012) that many hot Jupiters appear to have inflated radii. Proposed explanations involve the injection of some of the received stellar energy into the planet interior (Showman and Guillot 2002), but the exact mechanism remains disputed. Moreover, empirical evidence seems to suggest that stars hosting hot Jupiters have younger gyrochronological ages compared to their isochronal age estimates (Lanza 2010; Brown 2014; Maxted et al. 2015). This might be caused by a transfer of angular momentum from the massive, close-in planet to the star, causing a tidal spin-up, which results in the star rotating faster and, as a consequence, appearing younger than expected. The precise mechanism is, again, still unknown.

A larger sample of exoplanets is needed in order to solve the mysteries concerning the fascinating hot Jupiters and their curious behavior. However, it is still important to provide follow-up observations of the known transiting exoplanets. This allows to further constrain the planetary parameters and properly plan future observations with larger facilities in order to avoid wasting part of their observing time. As an example, the transit times of near future events are predicted with relatively good accuracy, while uncertainties cause a progressive degrade of the ephemeris accuracy as the time passes, due to the limited amount of available data for each planet and other issues, such as tidal orbital decay or gravitational interactions of the planet with other bodies. Follow-up observations of transiting hot Jupiters are therefore of fundamental importance to plan future observations.

This is the reason behind our choice to examine one such hot Jupiter. Orbiting around WASP-135 (1SWASPJ174908.40+295244.9), a Sun-like G5V star with $V = 13.28$ and $B - V = 0.97$ (Zacharias et al. 2022), WASP-135b was discovered by Spake et al. (2016), using photometric observations of the transit light curves performed by SuperWASP-N and NITES, and radial velocity measurements

with the SOPHIE spectrograph. The planet was characterized as a typical short-period ($P \simeq 1.401$ days) highly-irradiated hot Jupiter, with an inflated radius of $1.30 \pm 0.09\, R_{Jup}$ (from the transit light curve fitting) and a mass of $1.90 \pm 0.08\, M_{Jup}$ (from radial velocity). Moreover, an age discrepancy of the host star was found, the gyrochronological age being lower than the isochronal age: this was interpreted as a weak evidence of a transfer of angular momentum from the planet to its star.

We present here a new analysis of the transit light curves of WASP-135b, using data from two different datasets, one obtained from the TESS (Transiting Exoplanet Survey Satellite) space telescope, the other from the TASTE (The Asiago Search for Transit timing variation of Exoplanets) program at the Asiago Astrophysical Observatory.

1.1. Stellar parameters

In order to perform the complete analysis of the hot Jupiter WASP-135b, some knowledge of its hosting star is needed, in particular its effective temperature T_{eff}, metallicity $[Fe/H]$ and surface gravity $\log(g)$. These parameters will be used in the process of computing the limb darkening coefficients, and are retrieved from the literature. Since our analysis is solely based on photometric observations, we chose to consider only spectroscopical studies. In this way, the independence of the stellar parameters from photometric analyses was ensured. In particular, we used data from the discovery paper of our planet (Spake et al. 2016), since it provides the most precise and complete analysis of WASP-135. Spake et al. (2016) used spectra obtained with SOPHIE, a spectrograph mounted on the 1.93-m telescope of the Observatorie de Haute-Provence. In their work, the effective temperature was determined from the excitation balance of the Fe I lines, while the surface gravity was probed using the Na I D lines and the ionization balance of Fe I and Fe II. Lastly, the metallicity was obtained from the equivalent width measurements of several unblended lines. The final values, used in our analysis, are:

$$T_{eff} = (5680 \pm 60)\,\mathrm{K} \tag{1}$$

$$[Fe/H] = 0.02 \pm 0.13 \tag{2}$$

$$\log(g) = 4.50 \pm 0.10 \tag{3}$$

Moreover, we also used Spake et al. (2016) values for the stellar radius, mass and density as priors during the transit analysis with **PyORBIT**, namely: $R_S = (0.96 \pm 0.05)\, R_\odot$, $M_S = (0.98 \pm 0.06)\, M_\odot$, $\rho_S = (1.12 \pm 0.15)\, \rho_\odot$.

2. Observations

2.1. TESS

WASP 135b was observed by TESS's photometry instrument during sectors 26, 52, and 53 with observation dates respectively 9 June 2020, 19 May 2022, and 13 June 2022 in Year 2 and Year 4 observation missions. TESS filter in the optical band was used for all sectors for photometric analysis and limb darkening coefficient estimation.

We downloaded PDCSAP and SAP light curves from the *Milkowski Archive for Space Telescopes (MAST)*. Flux calculations were performed with their errors based on PDCSAP light curves of the three sectors. **wōtan** (Hippke et al. 2019) and **transitleastsquares** (Hippke and Heller 2019) packages were used respectively for light curve flattening and for searching transit-like features while taking the stellar limb darkening and planetary ingress and egress into account. We used the transit modeling package **batman** (Kreidberg 2015) and *Kipping transformations* for a limb darkening law selection for the sampling of the limb darkening coefficients.

Finally, light curve fitting was performed by Markov-Chain Monte Carlo (MCMC) algorithm and **PyORBIT** (Malavolta 2016) both for TESS and TASTE photometric analysis.

2.2. TASTE

TASTE is a project started by a group of scientists in 2009. The project aims to collect light curves of exoplanet transits by using imaging differential photometry at the Asiago 1.82 m telescope by applying a method used for detecting earth-sized exoplanets. The method is based on the timing analysis of a known transit and searching for variations in the transit duration or the center of the transit due to the third body perturbations, e.g. a second planet or an exomoon (Nascimbeni et al. 2011).

WASP 135b was observed (observer; Borsato) with Asiago 1.82 m reflector telescope under the "Nascimbeni" program with an observation date of 10 September 2021. The r-Sloan filter was used for the photometric analysis. Bias and flat corrections were applied with appropriate standard deviations and noise that are comparable to the expected values. The time manipulations were made for the Barycentric Julian Date (BJD) and the Barycentric Dynamical Time (TDB) using the **astropy.time** packet. Aperture photometry was applied using the *centroid algorithm* for the target and reference stars, in order to perform differential photometry.

3. Data reduction

3.1. TASTE data reduction

Data reduction of the TASTE dataset has been performed using the standard calibration of the science frames with bias and flat frames.

We used 30 bias images in order to compute a master bias, where the value of each pixel is obtained by finding the median value corresponding with each pixel across all the bias frames. The operations are performed using values in photoelectrons: the conversion from Analog to Digital Units (ADU) to photoelectrons (e^-) was performed multiplying by the GAIN, which, in our analysis, was 1.91 e^-/ADU. We also found a value of readout noise (RON) of 7.1 e^-. The error on the master bias was calculated using the Standard Deviation (STD) of the values of the pixels, obtaining $\sigma_{mb} = 1.89\, e^-$.

The subsequent flat field analysis was performed using 30 flat frames. These were shot by taking short exposures of a homogeneously-illuminated screen on the telescope dome. By observing the flat images, differences in the illumination were found, due to different responses of the individual pixels of the CCD, as well as due to a lack of a precise calibration of the lamp used to illuminate the screen. After the usual conversion to photoelectrons, each flat frame has been corrected by subtracting the master bias, and then normalized by dividing the corrected image by the median of all the corrected images. The normalization was necessary in order to compensate for the effect of the lamp calibration. Another median of these 30 normalized and bias-corrected flat field images was performed, thus obtaining

the master flat. The error on the master flat was obtained using:

$$\sigma_{mf} = \sqrt{\frac{\sum_{i=1}^{30} \sigma_i^2}{30}} \tag{4}$$

where the error on the single flat frame is:

$$\sigma_i = \frac{\sqrt{\sigma_{mb}^2 + RON^2 + F_i}}{F_{median}} \tag{5}$$

where F_i is the flux of the single bias-corrected flat image, which follows a Poissonian distribution (therefore the associated error is $\sqrt{F_i}$), and F_{median} is the flux of the median of the corrected flat images.

At this point, the results were used to correct the 2161 science frames. Each corrected science frame was obtained by subtracting the master bias to the uncorrected science frame, and then dividing by the master flat:

$$F_{corr} = \frac{F_{debiased}}{F_{mf}} = \frac{F_{science} - F_{mb}}{F_{mf}} \tag{6}$$

where $F_{mb}, F_{mf}, F_{science}, F_{debiased}$ and F_{corr} are the fluxes of the master bias, the master flat, the uncorrected science frame, the debiased science frame, and the corrected science frame respectively. The error for the debiased frames is:

$$\sigma_{debiased} = \sqrt{F_{debiased} + RON^2 + \sigma_{mb}^2} \tag{7}$$

where $F_{debiased}$ follows a Poissonian distribution. The error on the corrected science frame is, instead:

$$\sigma_{corr} = F_{corr} \sqrt{\left(\frac{\sigma_{debiased}}{F_{debiased}}\right)^2 + \left(\frac{\sigma_{mf}}{F_{mf}}\right)^2} \tag{8}$$

Finally, we performed a change of the time reference, from the Julian Date in Universal Time Coordinate (JD-UTC) to the Barycentric Dynamical Time (TDB), then correcting for the light travel time, i.e. the time required by the light to travel between the Earth and the barycenter of the Solar System. An example of a single corrected science frame is visible in *Figure 7*.

3.2. TESS data reduction

The images from the TESS dataset had been already pre-reduced by the TESS science team, using an automatic pipeline providing calibrated pixels, simple aperture photometry, aperture photometry corrected for systematic errors, stellar centroid and related errors. The resulting calibrated pixels and extracted light curves were stored in the MAST website, that we used to download the SAP (Simple Aperture Photometry) and the PDCSAP (Presearch Data Conditioned Simple Aperture Photometry) light curves. An example of these curves, discussed later, is shown in *Figure 1* for the sector 26.

4. Data Analysis

4.1. TESS Analysis

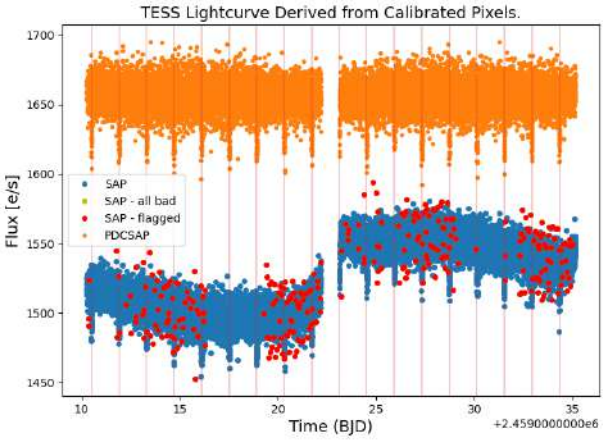

Fig. 1: TESS Lightcurves derived from Calibrated Pixels.

We downloaded SAP and PDCSAP light curves files from the MAST archive. The SAP lightcurves are aperture photometry flux series while PDCSAP lightcurves are the ones with removed instrumental systematics. PDCSAP is also corrected for the amount of flux captured by the photometric aperture and crowding from nearby stars. The same steps were applied for all three sectors for TESS analysis. The time was corrected to TESS BJD. Fluxes and their associated errors for SAP and PDCSAP were obtained. The plot of flux series for SAP and PDCSAP in units of e^-/s is given for Sector 26 in *Figure 1*, where *"SAP - all bad"* stands for quality flags of non-zero values and *"SAP - flagged"* for quality flags greater than or equal to 1.

We performed a fit on PDCSAP raw data to detrend the out-of-transit light curve in order to remove the trends affecting the flux, which are caused by stellar activity, stellar flares, gaps in the data, interrupted transits, etc. We used the **flatten** package from **wōtan** based on **biweight** method. Wōtan Comprehensive Time-series Detrending (Hippke et al. 2019) is a time-windowed slider with an iterative robust location estimator based on Tukey's biweight. Additionally, we included a spline-based method with a robust Huber estimator. The window length for biweight is 1.0 day while it is 0.8 days for Huber-spline. The plot of *"Out-of-transit Flattened Detrendending"* and *"Normalized Phase Transit"* based on the two methods can be seen in *Figure 2a* and *Figure 2b*. The resulting STDs for PDCSAP, biweight, and Huber-spline are respectively 0.007339, 0.007366, and 0.007333 e^-/s for sector 26. The corresponding values for sector 52 are 0.006512, 0.006774, 0.006822 e^-/s, for sector 53 are 0.005389, 0.005181, 0.005176 e^-/s, respectively.

Transit search and fit were performed through TLS (**transitleastsquares**; Hippke and Heller 2019) and BLS (**BoxLeastSquares**) from **astropy.timeseries**. Time series are given as periodograms, first for BLS and then for TLS. The results of the analyses are shown in figures *Figure 3a* and *Figure 3b*, respectively. The best results were obtained with the latter. For Sector 26 the output gave a period of 1.40131 d (days), a normalized flux at the center of transit of 0.98057 e^-/s, a best duration of 0.05714 d, and a signal detection efficiency (SDE) of 19.0275. These values are compared with the period of 1.4013788 d from Kokori et al. (2022). The plot of *"Fit of the*

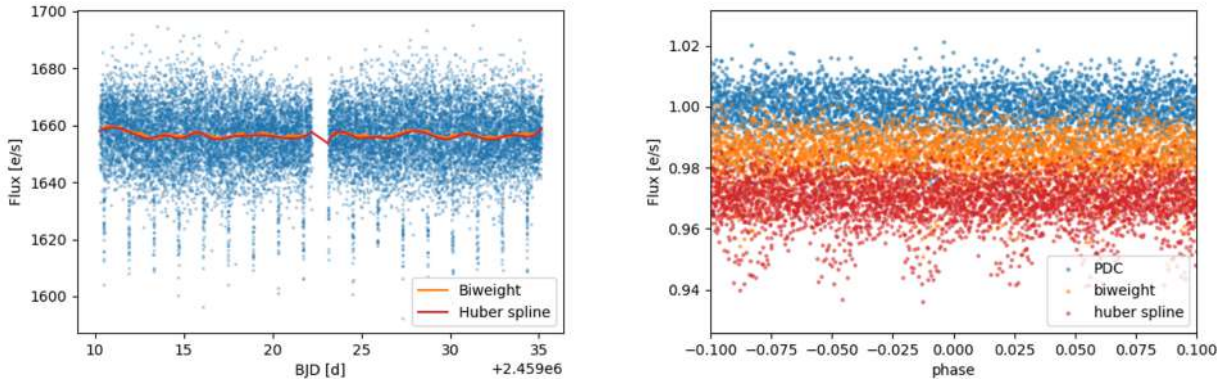

(a) (b)

Fig. 2: Detrending of the TESS data. (a) Out-of-transit Flattened Detrendending. (b) Normalized Phase Transit.

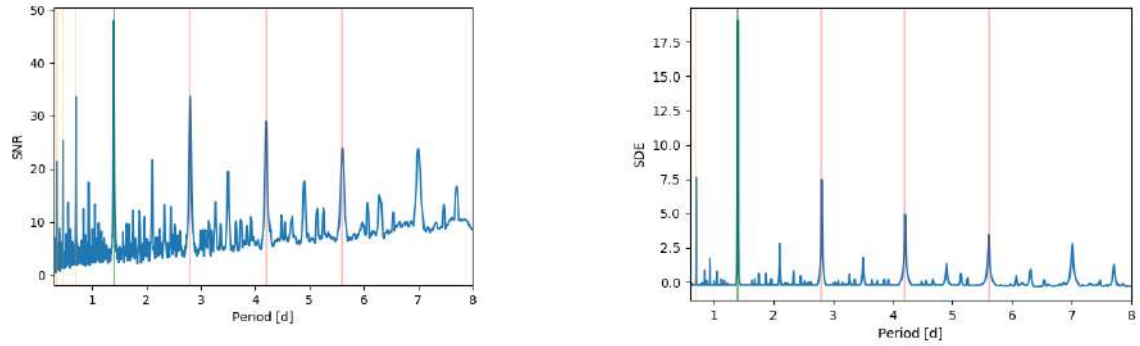

(a) (b)

Fig. 3: Transit detection for the TESS data. (a) Periodogram for BLS. (b) Periodogram for TLS.

phase-folded light curve for TESS data (Sector 26)", obtained with **transitleastsquares**, can be seen in *Figure 4*.

We used **ldtk** (*Limb Darkening Toolkit*, Parviainen and Aigrain 2015) package for stellar limb darkening calculations. **ldtk** is a python package using the library of **PHOENIX** for calculating stellar limb darkening profiles and model-specific limb darkening coefficients. Parametrization of coefficients was performed using a quadratic limb darkening law for the indensity of the flux $I(\mu)$, from Kipping (2013):

$$I(\mu)/I(1) = 1 - u_1(1-\mu) - u_2(1-\mu)^2 \tag{9}$$

where we have defined

$$q_1 = (u_1 + u_2)^2 \tag{10}$$

$$q_2 = \frac{u_1}{2(u_1+u_2)} \tag{11}$$

and $\mu = \sqrt{(1-r^2)}$ is connected to the normalized radial coordinate r, while $I(1)$ is the intensity when $\mu = 1$ (no limb darkening effect). The stellar parameters of WASP-135 used for modeling were taken from Spake et al. (2016). Limb darkening coefficients for TESS data, using the "TESS.Red" filter, were found to be $u_1 = 0.4241 \pm 0.0133, u_2 = 0.1332 \pm 0.0331$. Filter profiles were obtained from *Spanish Virtual Observatory (SVO) Filter Profile Service (FPS)*.

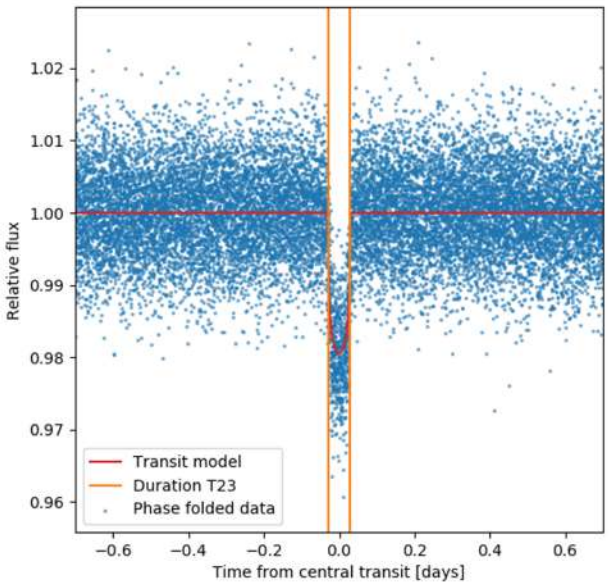

Fig. 4: Fit of the phase-folded light curve for TESS data (sector 26).

Parameters	TESS Analysis (this paper)	TASTE Analysis (this paper)	Spake et al. (2016)
Planetary parameters			
Orbital period [d]	1.401378 ± 10^{-6}	1.401378 ± 10^{-6}	$1.4013794 \pm 8 \times 10^{-7}$
Impact parameter [R_s]	0.69 ± 0.02	$0.66^{+0.02}_{-0.03}$	0.80 ± 0.03
Planetary radius [R_s]	0.138 ± 0.001	0.131 ± 0.002	
Planetary radius [R_{Jup}]	1.29 ± 0.07	1.23 ± 0.07	1.30 ± 0.09
Planetary radius [$R_\oplus$]	14.5 ± 0.8	13.7 ± 0.7	14.6 ± 1.0
Eccentricity (assumption)	0	0	0
Argument of periastron (assumption) [°]	90	90	90
Semi-major axis of the planet [R_s]	5.81 ± 0.13	5.97 ± 0.15	
Semi-major axis of the planet [AU]	0.0259 ± 0.0015	0.0260 ± 0.0015	0.0243 ± 0.0005
Inclination of the orbit [°]	83.19 ± 0.33	$83.64^{+0.38}_{-0.39}$	82.0 ± 0.6
Planetary mass [M_{Jup}]			1.90 ± 0.08
Planetary density [g/cm^3]	1.09 ± 0.42	1.28 ± 0.46	1.16 ± 0.23
Stellar parameters			
Stellar density [$\rho_\odot$]	1.34 ± 0.09	$1.45 \pm +0.11$	$1.12 \pm +0.15$
Limb darkening coefficient ld_{c1}	0.421 ± 0.013	0.519 ± 0.018	
Limb darkening coefficient ld_{c1}	$0.122^{+0.033}_{-0.032}$	0.116 ± 0.040	

Table 1: Results of the analysis of WASP-135b, from TESS and TASTE datasets. A comparison with the values in the discovery paper is also provided. The values of the eccentricity and of the argument of periastron are a consequence of the assumption of circular orbit. The values of the planetary density are just a rough estimate, obtained using the value of the planetary mass from Spake et al. (2016) and the planetary radius from our analysis.

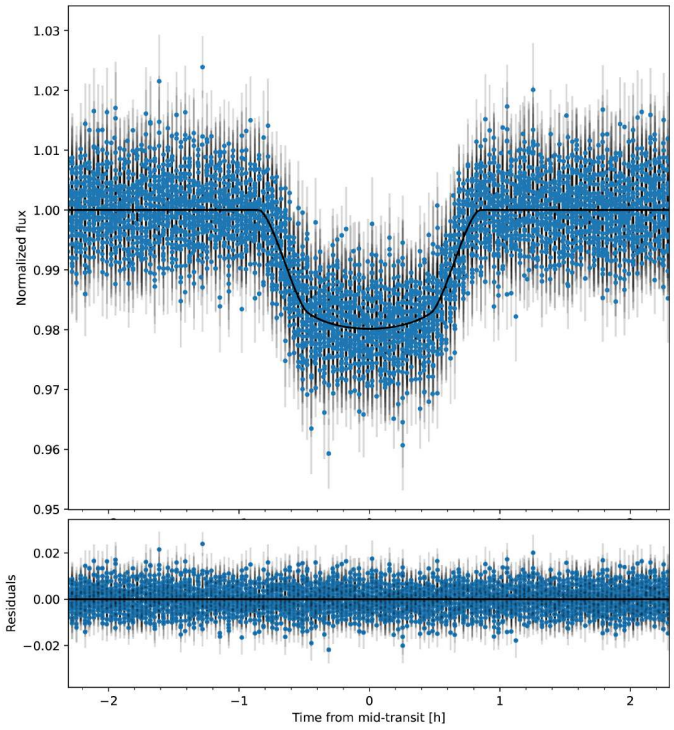

Fig. 5: TESS Light curve and Residuals (larger version of this plot in *Appendix A*).

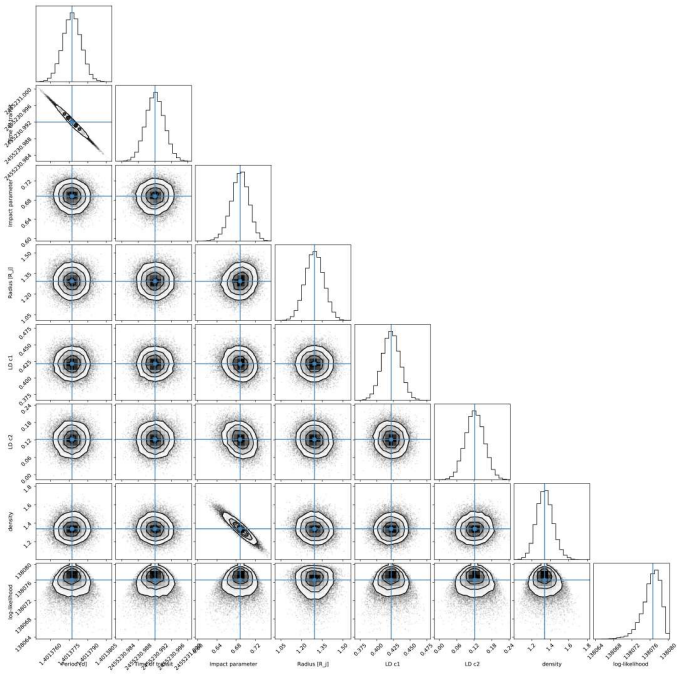

Fig. 6: TESS Corner Plot (larger version of this plot in *Appendix A*).

Finally, we created a configuration file including the models applied and parameters obtained from the analysis mentioned above. **batman_transit** model (Kreidberg 2015) was chosen for the light curve, and both the limb darkening parameters and the period were set as uniform priors. Due to the closeness of the planet to its hosting star, we assumed a circular orbit as a consequence of tidal circularization (Nagasawa et al. 2008). By using the configuration file, we ran **PyORBIT**, that uses a Markov-Chain Monte-Carlo (MCMC) sampler algorithm to produce the final modeling of the orbital fit and a corner plot showing the correlations between parameters. **PyORBIT** is a robust, versatile framework for the characterization of planetary systems and modeling light curves, radial velocities, activity indexes, and transit time variations.

A comparison of the orbital TESS parameters found in our analysis and Spake et al. (2016) is given in *Table 1*. The plotted final light curve with residuals using **gridspec** package and

the corner plot using **corner** package are respectively given in *Figure 5* and *Figure 6*.

In addition to the light curve and the corner plot obtained setting priors on limb darkening coefficients, we ran **PyORBIT** leaving limb darkening coefficients as free parameters. We compared the results between two fits and decided to use the results obtained only with setting priors, which performed better correlations between parameters and a more satisfying fit applied on the light curve. We end the TESS analysis here.

4.2. TASTE Analysis

As mentioned before, the TASTE project aims to have a differential photometry analysis of the host star. This method is applied by the flux measurements and their associated errors within a selected annulus with inner and outer radii defined for both target and reference stars. The plot of the target star in the same frame as the selected reference star can be seen in *Figure 7*.

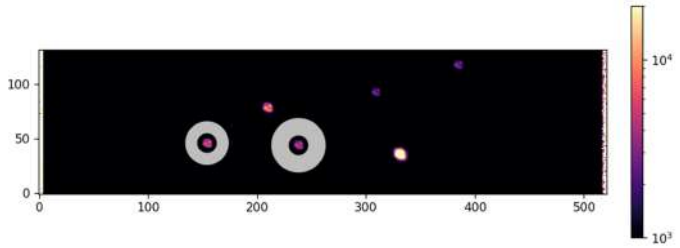

Fig. 7: Example of a corrected science frame from TASTE. On the left the reference star, on the right the target star.

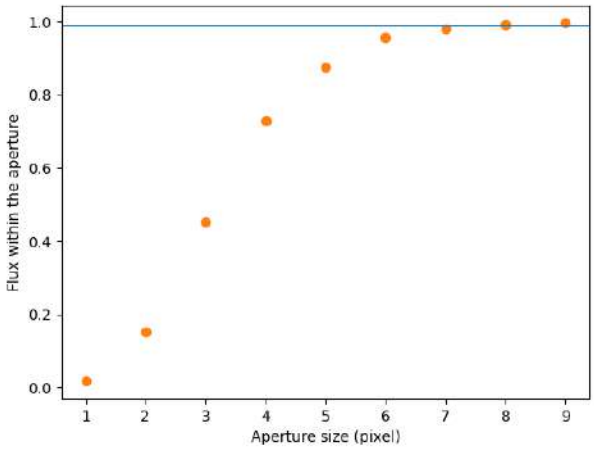

Fig. 8: Integrated flux of the reference star as a function of the aperture, for TASTE data.

Reference stars used for aperture photometry are chosen with similar intensity with respect to the target star, and not saturating the CCD. We selected circular sky annuli both around the target and reference stars, with an outer radius of 15 pixels and an inner radius of 8 pixels, using **Circle** package from **matplotlib.patches**. We computed the flux of the target star in the inner radius of the annulus in units of photons/pixel with its associated error by using the centroid algorithm in order to obtain the refined pixel coordinates of the target star. We computed the photocenter of the target and of the reference stars and applied aperture photometry for each of them. The choice of an inner radius of 8 pixels was made in order to retain the 99% of the flux of the star. In fact, in *Figure 8*, the integrated flux as a function of the aperture for the reference star is shown. The flux within the aperture should flatten out in an asymptotic way as the entire point-spread function of the star is enclosed within the aperture and only sky background continues to contribute.

At this point, by using the refined coordinates, we computed the sky flux in units of photons/pixel and its associated error, the first being the mean flux within the annulus, and the second being given by:

$$\sigma_{sky} = \frac{\sqrt{\sum_{sky} \sigma^2_{sky}}}{N_{sky}} \tag{12}$$

where *sky* indicates the position of the particular pixel inside the annulus and N_{sky} indicates the number of pixels within the annulus. The flux of a star (target or reference) is obtained by subtracting the flux of the sky inside the aperture (inner radius) to the measured total flux in the same area.

Finally, differential photometry was applied by dividing the aperture photometry of the target star by the aperture photometry of one of the reference stars. The associated error was estimated using:

$$\sigma_{dp} = F_{dp} \sqrt{\left(\frac{\sigma_{target}}{F_{target}}\right)^2 + \left(\frac{\sigma_{reference}}{F_{reference}}\right)^2} \tag{13}$$

where F_{dp}, F_{target} and $F_{reference}$ are the fluxes of differential photometry, target star and reference star respectively, while σ_{dp}, σ_{target} and $\sigma_{reference}$ are the corresponding errors. The resulting light curve of the transit was obtained plotting the flux of the target star, rescaled from differential photometry, as a function of the time in BJD.

From **numpy.polynomial.polynomial** we used the **polyfit** packet to generate coefficients which were used in modeling a light curve to fit the data and the **polyval** package to evaluate a polynomial for a set of transit time in *bjd_tdb*. We applied the **polynomalpolyfit** curve fitting model to the light curve obtained with differential photometry as a function of transit time in *bjd_tdb*. Out-of-transit STD was found to be 0.00509.

Limb darkening parametrization was applied in the same way as in TESS analysis, using Kipping transformations for quadratic law with stellar parameters obtained from Spake et al. (2016). *sloan_r* filter was used for TASTE data, and the coefficients were found to be $u_1 = 0.5262 \pm 0.0184, u_2 = 0.1358 \pm 0.0404$.

We performed an orbital fit of the TASTE light curve with **PyORBIT**, using in the MCMC the orbital period obtained from the final TESS fit as a prior in the new configuration file with a Gaussian prior. In fact, since TASTE data covers a single transit, it provides no information about the orbital period. The new limb darkening coefficients were set as a Gaussian prior around the derived values for *c1* and *c2*, with $\sigma = 0.10$. The light curve model followed the model in the TESS configuration file. The final fit of the differential and normalized light curves with residuals and the corner plot can be seen in *Figure 9* and *Figure 10*. A comparison of the orbital TASTE parameters found in our analysis with (Spake et al. 2016) is given in *Table 1*.

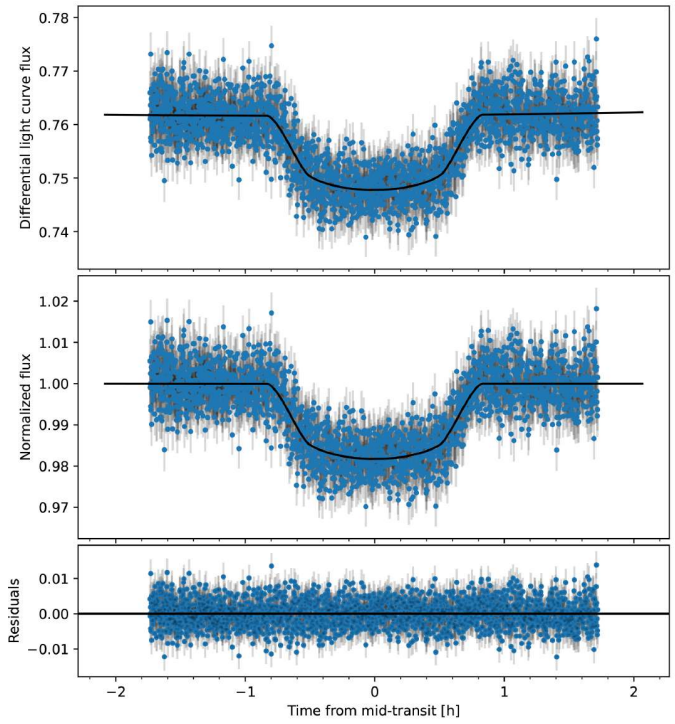

Fig. 9: TASTE Differential & Normalized Light curve and Residuals (larger version of this plot in *Appendix A*).

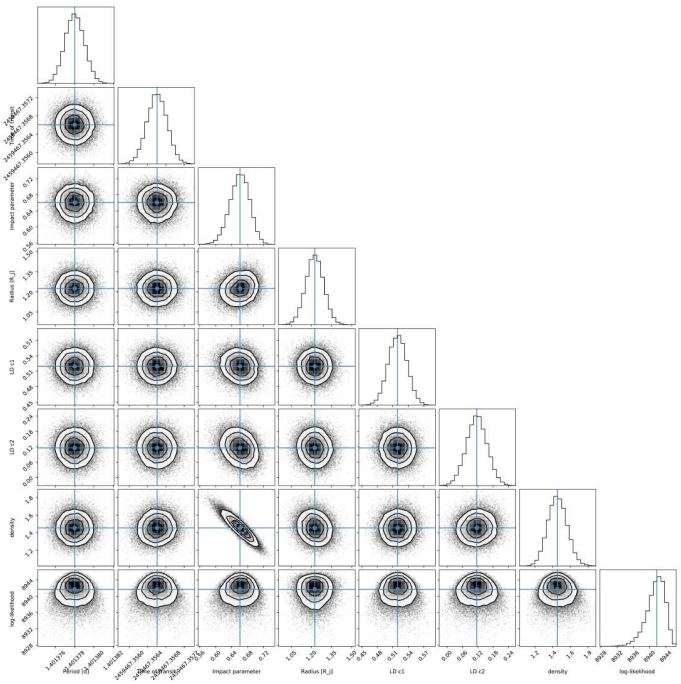

Fig. 10: TASTE Corner Plot (a larger version of this plot in *Appendix A*).

As mentioned before, the orbital period used in the TASTE fit was taken from the TESS fit applied by **PyORBIT**. Different priors set in the TESS configuration file directly affect the results of the TASTE fit, as well as priors set in the TASTE configuration file itself. The analysis until this point was made using both TESS and TASTE fits with priors on the limb darkening coefficients, using the models and laws previously discussed. In addition to the fit performed via setting priors on limb darkening (LD) coefficients, we also experimented with other fits made with none-set priors on the coefficients, combining:

1. LD priors set TESS fit with none-set LD priors TASTE fit,
2. none-set LD priors TESS fit and none-set LD priors TASTE fit, and finally
3. none-set LD priors TESS fit and LD priors set TASTE fit.

The best correlations and results were reached via a combination of TESS and TESS analysis both with priors on limb darkening coefficients. We conclude the analysis of our research here.

5. Discussion and conclusions

Two transit light curves from TESS and TASTE were analyzed to measure the transit of WASP-135b past its host star. Parameters for both the planet and star were found for both light curves and reported in *Table 1*, as well as values from the discovery paper. Values of parameters found from TESS and TASTE data can then be compared to other values of parameters from the literature, with the parameters of greatest interest being orbital period and radius of the exoplanet.

These values were found to be $P = (1.401378 \pm 0.000001)$ d and $R = (1.293538 \pm 0.07)\, R_{Jup}$ for TESS, and $P = (1.401378 \pm 0.000001)$ d and $R = (1.225463 \pm 0.07)\, R_{Jup}$ for TASTE. The values from the literature are $P = (1.4013794 \pm 0.0000008)$ d and $R = (1.30 \pm 0.09)\, R_{Jup}$ (Spake et al. 2016), $P = (1.4013795^{+0.0000007}_{-0.0000008})$ d (Patel and Espinoza 2022), $P = (1.40137841 \pm 0.00000034)$ d (Ivshina and Winn 2022), and $P = (1.4013788 \pm 0.0000004)$ d (Kokori et al. 2022).

All values of orbital period found from TESS and TASTE data and those from the literature were found to have overlapping error bars, with the largest variation between two reported periods being 0.0000015d $\sim$ 0.13s, with errors as large as 0.000001d $\sim$ 0.086s. These negligible differences in period across different measurements of the planet's period indicate a low variation in the planet's period, which could be used to place bounds on any natural precession of the orbit of WASP-135b, or the orbital parameters of any other potential exoplanets or exomoons in the WASP-135 system in future work.

The TESS and TASTE planetary radius values and the value of planetary radius from Spake et al. (2016) also all have overlapping error bars. The value from TASTE was less consistent with the other two values than they were with each other, although it is not clear from the values found which is likely to be closer to the true value of the planetary radius. It is possible that quality issues with TASTE caused it to not agree as strongly with the other two values as it could have, although it cannot be ruled out that TASTE made the more accurate measurement. The fact that the TESS and TASTE data were processed in nearly the same way indicates that the data processing performed on the two data sets is likely not a major source of the discrepancy between the measured values.

Our purely photometric analysis cannot provide values for planetary mass and density. Nevertheless, a rough estimate of the planetary density can be obtained using the value of the planetary mass from Spake et al. (2016), namely $(1.90 \pm 0.08)\, M_{Jup}$, and the values of the planetary radius from our analysis. In this way, we obtain a value of $\rho = (1.09 \pm 0.42)$ g/cm^3 from TESS data,

and of $\rho = (1.28 \pm 0.46)\,\mathrm{g/cm^3}$ from TASTE data. Both these values agree with the value provided by the discovery paper, and moreover confirm the idea that WASP-135b shows an inflated radius, a typical feature of many short-period highly-irradiated hot Jupiters.

Overall it can be reported that the parameters found for WASP-135b from the TESS and TASTE data are compatible with those already found in the previous papers that examined this planetary system. The parameters found here are also the most extensive set of parameters for the system other than what was reported in Spake et al. (2016) in the initial discovery of WASP-135b. This investigation of the WASP-135 system can be used as part of future work to better examine this system to learn more about these hot Jupiters and exoplanets in general.

References

I. Baraffe, G. Chabrier, and T. Barman. The physical properties of extra-solar planets. *Reports on Progress in Physics*, 73(1):016901, dec 2009. . URL https://doi.org/10.1088%2F0034-4885%2F73%2F1%2F016901.

K. Batygin and M. E. Brown. EVIDENCE FOR a DISTANT GIANT PLANET IN THE SOLAR SYSTEM. *The Astronomical Journal*, 151(2):22, jan 2016. . URL https://doi.org/10.3847%2F0004-6256%2F151%2F2%2F22.

C. Beaugé and D. Nesvorný. MULTIPLE-PLANET SCATTERING AND THE ORIGIN OF HOT JUPITERS. *The Astrophysical Journal*, 751(2):119, may 2012. . URL https://doi.org/10.1088%2F0004-637x%2F751%2F2%2F119.

D. J. A. Brown. Discrepancies between isochrone fitting and gyrochronology for exoplanet host stars? *Monthly Notices of the Royal Astronomical Society*, 442 (2):1844–1862, jun 2014. . URL https://doi.org/10.1093%2Fmnras%2Fstu950.

J. J. Fortney and N. Nettelmann. The interior structure, composition, and evolution of giant planets. *Space Science Reviews*, 152(1-4):423–447, dec 2009. . URL https://doi.org/10.1007%2Fs11214-009-9582-x.

M. Hippke and R. Heller. Optimized transit detection algorithm to search for periodic transits of small planets. *Astronomy &amp Astrophysics*, 623:A39, feb 2019. . URL https://doi.org/10.1051%2F0004-6361%2F201834672.

M. Hippke, T. J. David, G. D. Mulders, and R. Heller. ttwōtan/tt: Comprehensive time-series detrending in python. *The Astronomical Journal*, 158(4):143, sep 2019. . URL https://doi.org/10.3847%2F1538-3881%2Fab3984.

E. S. Ivshina and J. N. Winn. TESS transit timing of hundreds of hot jupiters. *The Astrophysical Journal Supplement Series*, 259(2):62, apr 2022. . URL https://doi.org/10.3847%2F1538-4365%2Fac545b.

D. M. Kipping. Efficient, uninformative sampling of limb darkening coefficients for two-parameter laws. *Monthly Notices of the Royal Astronomical Society*, 435(3):2152–2160, aug 2013. . URL https://doi.org/10.1093%2Fmnras%2Fstt1435.

W. Kley and R. Nelson. Planet-disk interaction and orbital evolution. *Annual Review of Astronomy and Astrophysics*, 50(1):211–249, sep 2012. . URL https://doi.org/10.1146%2Fannurev-astro-081811-125523.

A. Kokori, A. Tsiaras, B. Edwards, A. Jones, G. Pantelidou, G. Tinetti, L. Bewersdorff, A. Iliadou, Y. Jongen, G. Lekkas, A. Nastasi, E. Poultourtzidis, C. Sidiropoulos, F. Walter, A. Wünsche, R. Abraham, V. K. Agnihotri, R. Albanesi, E. Arce-Mansego, D. Arnot, M. Audejean, C. Aumasson, M. Bachschmidt, G. Baj, P. R. Barroy, A. A. Belinski, D. Bennett, P. Benni, K. Bernacki, L. Betti, A. Biagini, P. Bosch, P. Brandebourg, L. Brát, M. Bretton, S. M. Brincat, S. Brouillard, A. Bruzas, A. Bruzzone, R. A. Buckland, M. Caló, F. Campos, A. Carreno, J. A. C. Rodrigo, R. Casali, G. Casalnuovo, M. Cataneo, C. M. Chang, L. Changeat, V. Chowdhury, R. Ciantini, M. Cilluffo, J. F. Coliac, G. Conzo, M. Correa, G. Coulon, N. Crouzet, M. V. Crow, I. Curtis, D. Daniel, S. Dawes, B. Dauchet, M. Deldem, D. Deligeorgopoulos, G. Dransfield, R. Dymock, T. Eenmäe, P. Evans, N. Esseiva, C. Falco, R. G. Farfán, E. Fernández-Lajús, S. Ferratfiat, S. L. Ferreira, A. Ferretti, J. Fiołka, M. Fowler, S. R. Futcher, D. Gabellini, T. Gainey, J. Gaitan, P. Gajdoš, A. García-Sánchez, J. Garlitz, C. Gillier, C. Gison, F. G. Horta, G. Grivas, J. Gonzales, D. Gorshanov, P. Guerra, T. Guillot, C. A. Haswell, T. Haymes, V. P. Hentunen, K. Hills, K. Hose, T. Humbert, F. Hurter, T. Hynek, M. Irzyk, J. Jacobsen, A. L. Jannetta, K. Johnson, P. Jóźwik-Wabik, A. E. Kaeouach, W. Kang, H. Kiiskinen, T. Kim, Kivila, B. Koch, U. Kolb, H. Kučáková, S. P. Lai, D. Laloum, S. Lasota, L. A. Lewis, G. I. Liakos, F. Libotte, C. Lopresti, F. Lomoz, R. Majewski, A. Malcher, M. Mallonn, M. Mannucci, A. Marchini, J. M. Mari, A. Marino, G. Marino, J. C. Mario, J. B. Marquette, F. A. Martínez-Bravo, M. Mašek, P. Matassa, P. Michel, J. Michelet, M. Miller, E. Miny, T. Mollier, D. Molina, B. Monteleone, N. Montigiani, M. Morales-Aimar, F. Mortari, M. Morvan, L. V. Mugnai, G. Murawski, L. Naponiello, R. Naves, J. L. Naudin, D. Néel, R. Neito, S. Neveu, A. Noschese, Y. Öğmen, O. Ohshima, Z. Orbanic, E. P. Pace, C. Pantacchini, N. I. Paschalis, C. Pereira, I. Peretto, V. Perroud, M. Phillips, P. Pintr, J. B. Pioppa, J. Plazas, A. J. Poelarends, A. Popowicz, J. Purcell, N. Quinn, M. Raetz, D. Rees, F. Regembal, M. Rocchetto, P. F. Rocci, M. Rockenbauer, R. Roth, L. Rousselot, X. Rubia, N. Ruocco, E. Russo, M. Salisbury, F. Salvaggio, A. Santos, J. Savage, F. Scaggiante, D. Sedita, S. Shadick, A. F. Silva, N. Sioulas, V. Školník, M. Smith, M. Smolka, A. Solmaz, N. Stanbury, D. Stouraitis, T. G. Tan, M. Theusner, G. Thurston, F. P. Tifner, A. Tomacelli, A. Tomatis, J. Trnka, M. Tylšar, P. Valeau, J. P. Vignes, A. Villa, A. V. Sureda, K. Vora, M. Vrašťák, D. Walliang, B. Wenzel, D. E. Wright, R. Zambelli, M. Zhang, and M. Zíbar. Exoclock project iii: 450 new exoplanet ephemerides from ground and space observations, 2022. URL https://arxiv.org/abs/2209.09673.

L. Kreidberg. ttbatman/tt: BAsic transit model cAlculatioN in python. *Publications of the Astronomical Society of the Pacific*, 127(957):1161–1165, nov 2015. . URL https://doi.org/10.1086%2F683602.

A. F. Lanza. Stellar activity, differential rotation, and exoplanets. *Proceedings of the International Astronomical Union*, 6(S273):89–95, aug 2010. . URL https://doi.org/10.1017%2Fs1743921311015067.

L. Malavolta. Pyorbit: Exoplanet orbital parameters and stellar activity. *Astrophysics Source Code Library*, dec 2016.

P. F. L. Maxted, A. M. Serenelli, and J. Southworth. Comparison of gyrochronological and isochronal age estimates for transiting exoplanet host stars. *Astronomy &amp Astrophysics*, 577:A90, may 2015. . URL https://doi.org/10.1051%2F0004-6361%2F201525774.

M. Mayor and D. Queloz. A jupiter-mass companion to a solar-type star. 378 (6555):355–359, nov 1995. . URL https://doi.org/10.1038/378355a0.

M. Nagasawa, S. Ida, and T. Bessho. Formation of hot planets by a combination of planet scattering, tidal circularization, and the kozai mechanism. *The Astrophysical Journal*, 678(1):498–508, may 2008. . URL https://doi.org/10.1086%2F529369.

S. Naoz, W. M. Farr, Y. Lithwick, F. A. Rasio, and J. Teyssandier. Secular dynamics in hierarchical three-body systems. *Monthly Notices of the Royal Astronomical Society*, 431(3):2155–2171, mar 2013. . URL https://doi.org/10.1093%2Fmnras%2Fstt302.

V. Nascimbeni, G. Piotto, L. R. Bedin, M. Damasso, L. Malavolta, and L. Borsato. TASTE II. a new observational study of transit time variations in HAT-p-13b. *Astronomy &amp Astrophysics*, 532:A24, jul 2011. . URL https://doi.org/10.1051%2F0004-6361%2F201116830.

H. Parviainen and S. Aigrain. ldtk: Limb darkening toolkit. *Monthly Notices of the Royal Astronomical Society*, 453(4):3822–3827, sep 2015. . URL https://doi.org/10.1093%2Fmnras%2Fstv1857.

J. A. Patel and N. Espinoza. Empirical limb-darkening coefficients and transit parameters of known exoplanets from TESS. *The Astronomical Journal*, 163 (5):228, apr 2022. . URL https://doi.org/10.3847%2F1538-3881%2Fac5f55.

A. P. Showman and T. Guillot. Atmospheric circulation and tides of "51 pegasus b-like" planets. *Astronomy &amp Astrophysics*, 385(1):166–180, apr 2002. . URL https://doi.org/10.1051%2F0004-6361%3A20020101.

J. J. Spake, D. J. A. Brown, A. P. Doyle, G. Hé brard, J. McCormac, D. J. Armstrong, D. Pollacco, Y. G. M. Chew, D. R. Anderson, S. C. C. Barros, F. Bouchy, P. Boumis, G. Bruno, A. C. Cameron, B. Courcol, G. R. Davies, F. Faedi, C. Hellier, J. Kirk, K. W. F. Lam, A. Liakos, T. Louden, P. F. L. Maxted, H. P. Osborn, E. Palle, J. P. Arranz, S. Udry, S. R. Walker, R. G. West, and P. J. Wheatley. WASP-135b: A highly irradiated, inflated hot jupiter orbiting a g5v star. *Publications of the Astronomical Society of the Pacific*, 128(960):024401, jan 2016. . URL https://doi.org/10.1088%2F1538-3873%2F128%2F960%2F024401.

D. S. Spiegel and A. Burrows. SPECTRAL AND PHOTOMETRIC DIAGNOSTICS OF GIANT PLANET FORMATION SCENARIOS. *The Astrophysical Journal*, 745(2):174, jan 2012. . URL https://doi.org/10.1088%2F0004-637x%2F745%2F2%2F174.

N. Zacharias, V. V. Makarov, C. T. Finch, H. C. Harris, J. A. Munn, and J. P. Subasavage. USNO bright star catalog, version 1. *The Astronomical Journal*, 164(2):36, jul 2022. . URL https://doi.org/10.3847%2F1538-3881%2Fac686d.

6. Appendix A - Figures

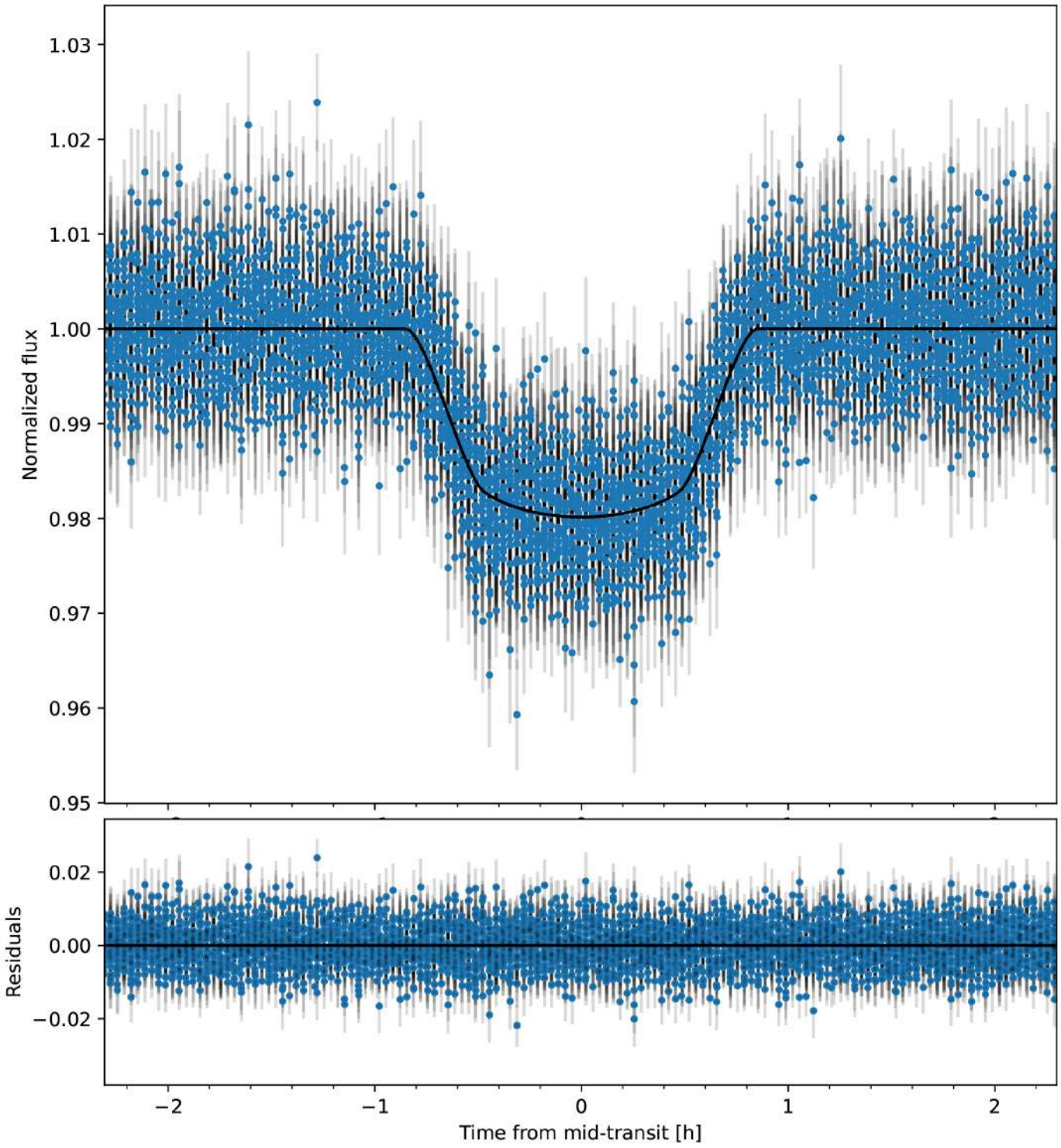

Fig. 5: TESS Light curve and Residuals.

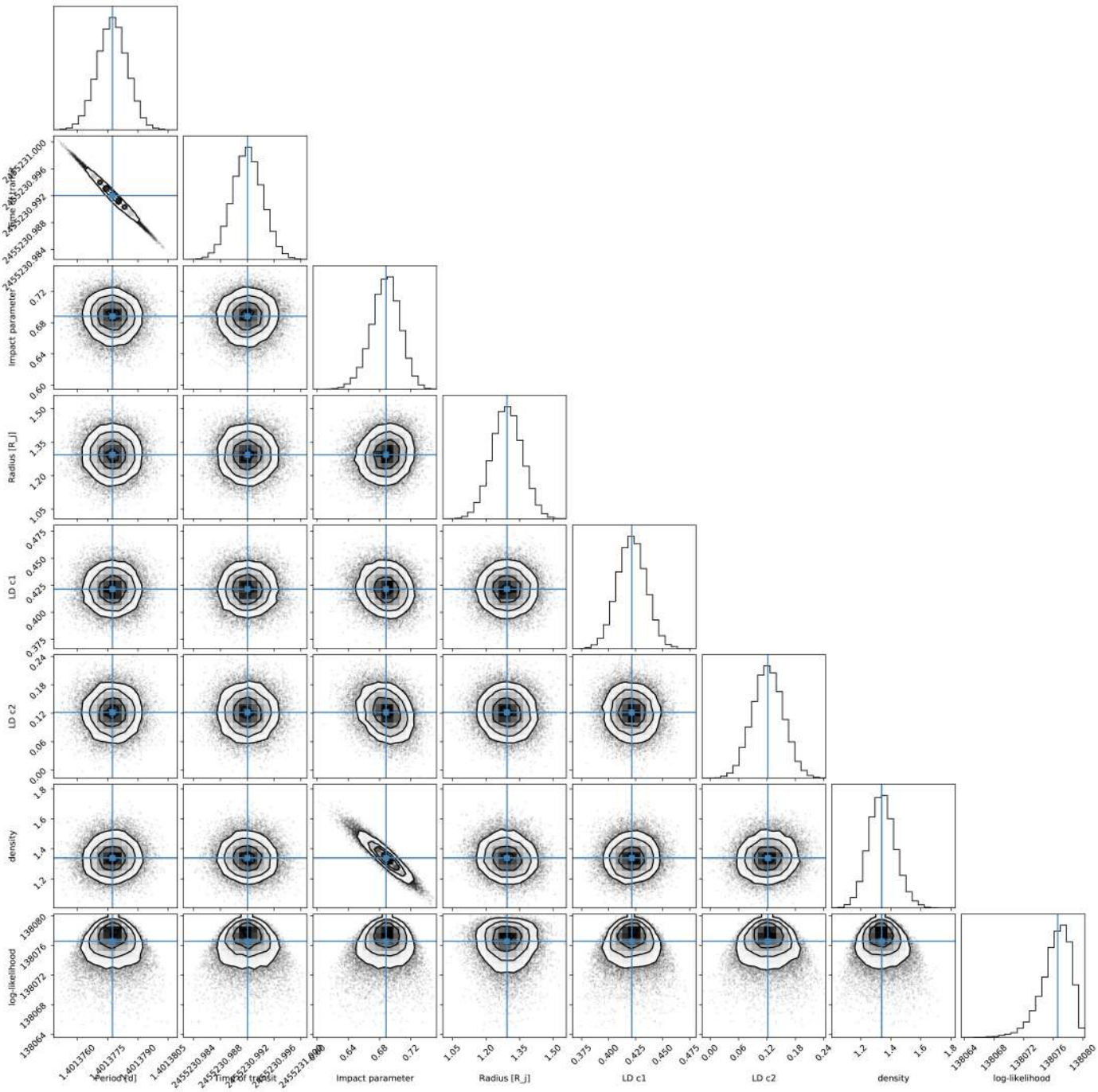

Fig. 6: TESS Corner Plot.

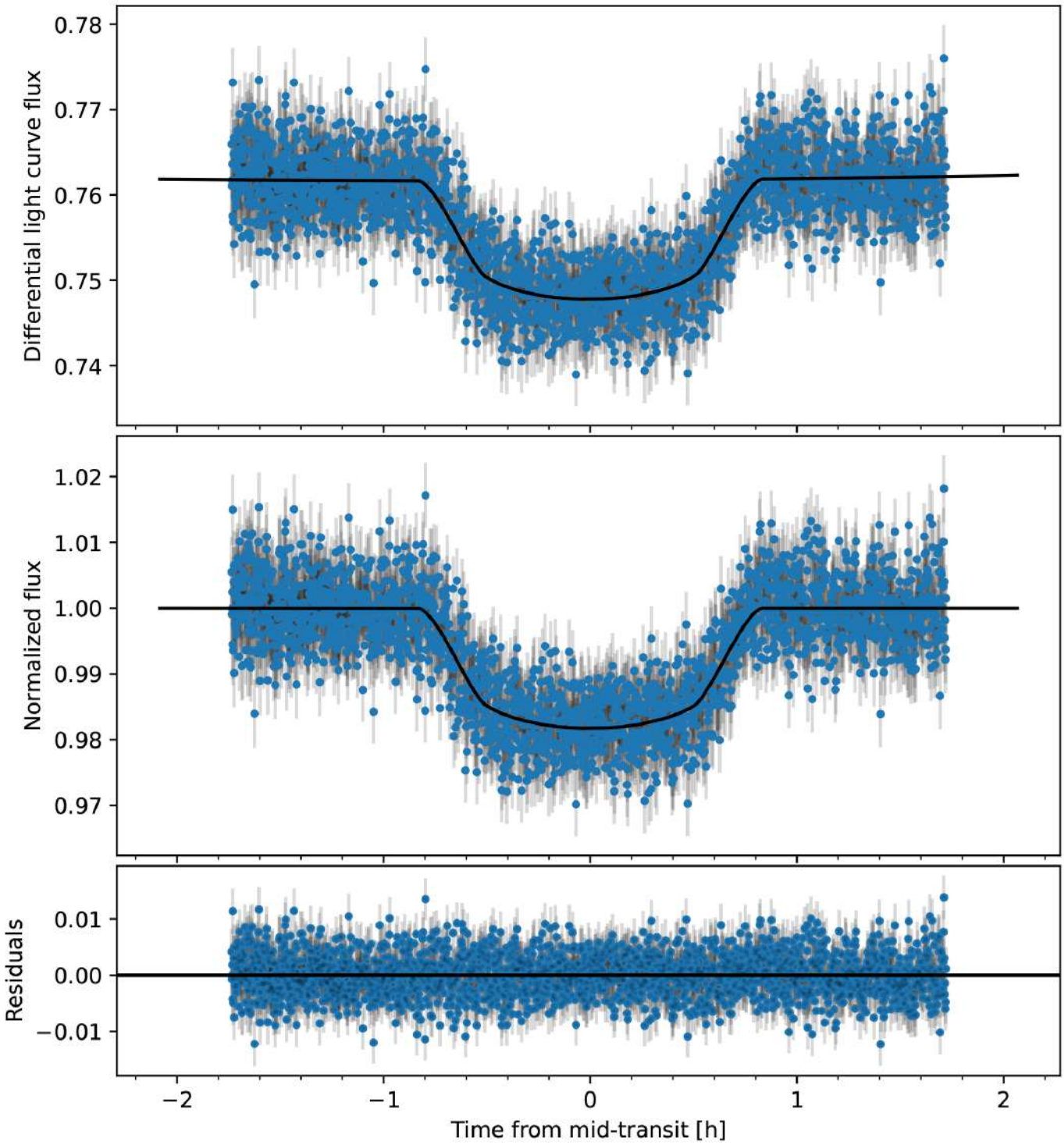

Fig. 9: TASTE Differential & Normalized Light curve and Residuals.

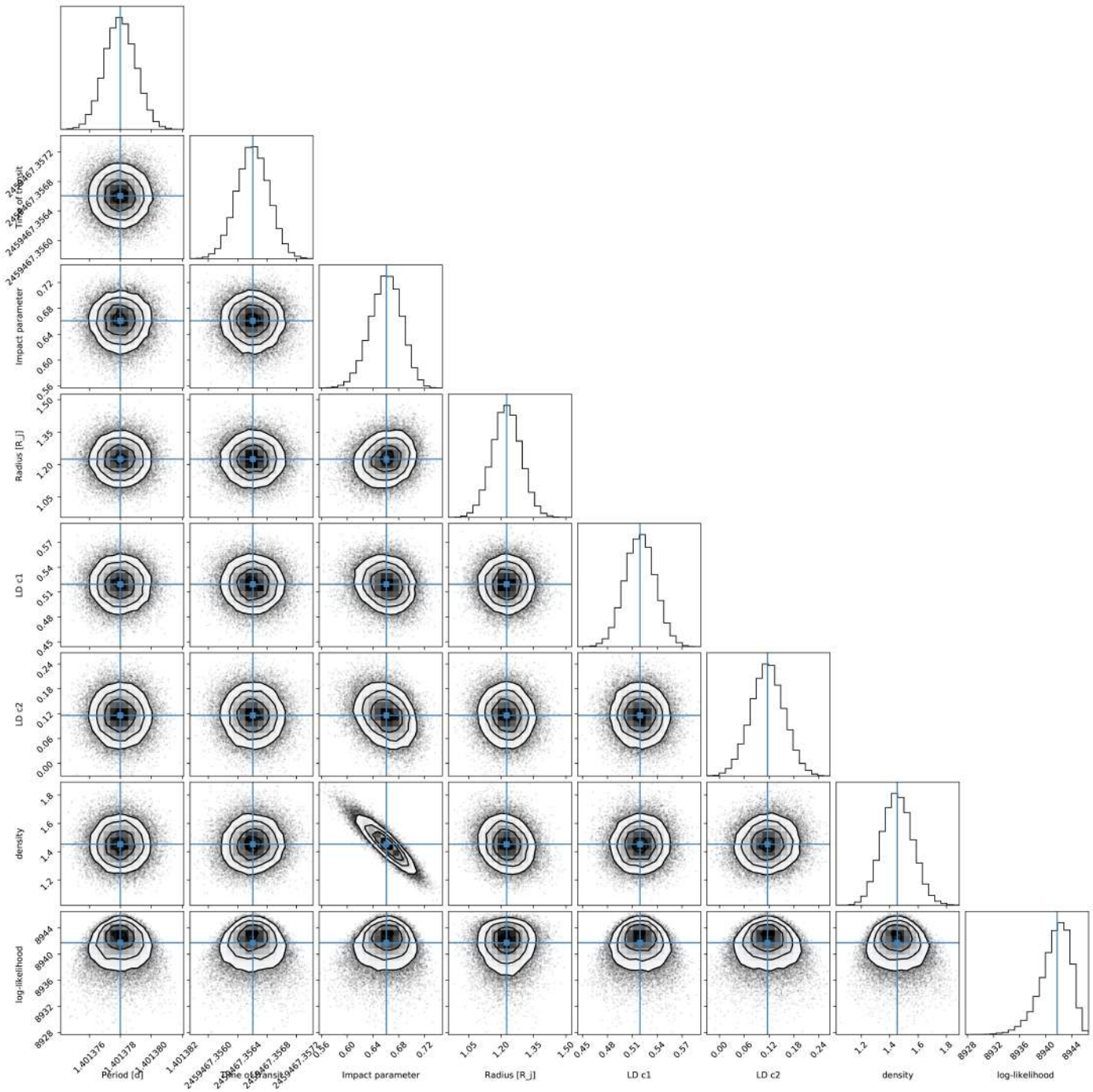

Fig. 10: TASTE Corner Plot.